The dynamic evolution of multipoint interplanetary coronal mass ejections observed with BepiColombo, Tianwen-1, and MAVEN

Chi, Y. ORCID: https://orcid.org/0000-0001-9315-4487, Shen, C. ORCID: https://orcid.org/0000-0002-3577-5223, Liu, J. ORCID: https://orcid.org/0009-0006-7051-0438, Zhong, Z. ORCID: https://orcid.org/0000-0002-5627-2377, Owens, M. ORCID: https://orcid.org/0000-0003-2061-2453, Scott, C. ORCID: https://orcid.org/0000-0001-6411-5649, Barnard, L. ORCID: https://orcid.org/0000-0001-9876-4612, Yu, B. ORCID: https://orcid.org/0000-0003-2758-1960, Heyner, D., Auster, H.-U., Richter, I. ORCID: https://orcid.org/0000-0002-5324-4039, Wang, Y. ORCID: https://orcid.org/0000-0002-8887-3919, Zhang, T., Guo, J. ORCID: https://orcid.org/0000-0002-8707-076X, Sánchez-Cano, B. ORCID: https://orcid.org/0000-0003-0277-3253, Pan, Z., Zou, Z. ORCID: https://orcid.org/0009-0008-9920-9600, Xu, M. ORCID: https://orcid.org/0000-0002-2924-7520, Cheng, L. ORCID: https://orcid.org/0000-0003-0578-6244, Su, Z. ORCID: https://orcid.org/0000-0001-5577-4538, Mao, D., Zhang, Z., Wang, C. ORCID: https://orcid.org/0000-0002-2865-4626, Wu, Z., Wang, G. ORCID: https://orcid.org/0000-0002-6618-4928, Xiao, S., Liu, K. ORCID: https://orcid.org/0000-0003-2573-1531, Hao, X., Li,

The Astrophysical Journal Letters, 951:L14 (10pp), 2023 July 1 https://doi.org/10.3847/2041-8213/acd7e7

The Dynamic Evolution of Multipoint Interplanetary Coronal Mass Ejections Observed with BepiColombo, Tianwen-1, and MAVEN

Yutian Chi[1], Chenglong Shen[2,3], Junyan Liu[4], Zhihui Zhong[4], Mathew Owens[5], Christopher Scott[5], Luke Barnard[5], Bingkun Yu[1], Daniel Heyner[6], Hans-Ulrich Auster[6], Ingo Richter[6], Yuming Wang[2,3,7], Tielong Zhang[3,8], Jingnan Guo[2,3], Beatriz Sánchez-Cano[9], Zonghao Pan[2,3], Zhuxuan Zou[4], Mengjiao Xu[1], Long Cheng[4], Zhenpeng Su[2,3], Dongwei Mao[4], Zhiyong Zhang[4], Can Wang[4], Zhiyong Wu[4], Guoqiang Wang[10], Sudong Xiao[10], Kai Liu[2,3], Xinjun Hao[2,3], Yiren Li[2,3], Manming Chen[2,3], and Mike Lockwood[5]

[1] Institute of Deep Space Sciences, Deep Space Exploration Laboratory, Hefei 230026, People's Republic of China
[2] Deep Space Exploration Laboratory/School of Earth and Space Sciences, University of Science and Technology of China, Hefei 230026, People's Republic of China; clshen@ustc.edu.cn
[3] CAS Center for Excellence in Comparative Planetology, University of Science and Technology of China, Hefei, People's Republic of China
[4] CAS Key Laboratory of Geospace Environment, Department of Geophysics and Planetary Sciences, University of Science and Technology of China, Hefei, People's Republic of China
[5] Department of Meteorology, University of Reading, Berkshire, UK
[6] Institut für Geophysik und extraterrestrische Physik, Technische Universität Braunschweig, Braunschweig, Germany
[7] Anhui Mengcheng Geophysics National Observation and Research Station, University of Science and Technology of China, Mengcheng, Anhui, People's Republic of China
[8] Space Research Institute, Austrian Academy of Sciences, Graz, Austria
[9] School of Physics and Astronomy, University of Leicester, Leicester, UK
[10] Institute of Space Science and Applied Technology, Harbin Institute of Technology, Shenzhen, People's Republic of China
Received 2023 March 21; revised 2023 April 18; accepted 2023 April 26; published 2023 June 29

Abstract

We present two multipoint interplanetary coronal mass ejections (ICMEs) detected by the Tianwen-1 and Mars Atmosphere and Volatile Evolution spacecraft at Mars and the BepiColombo (0.56 au ∼0.67 au) upstream of Mars from 2021 December 5 to 31. This is the first time that BepiColombo is used as an upstream solar wind monitor ahead of Mars and that Tianwen-1 is used to investigate the magnetic field characteristics of ICMEs at Mars. The Heliospheric Upwind Extrapolation time model was used to connect the multiple in situ observations and the coronagraph observations from STEREO/SECCHI and SOHO/LASCO. The first fast coronal mass ejection event (∼761.2 km s^{-1}), which erupted on December 4, impacted Mars centrally and grazed BepiColombo by its western flank. The ambient slow solar wind decelerated the west flank of the ICME, implying that the ICME event was significantly distorted by the solar wind structure. The second slow ICME event (∼390.7 km s^{-1}) underwent an acceleration from its eruption to a distance within 0.69 au and then traveled with the constant velocity of the ambient solar wind. These findings highlight the importance of background solar wind in determining the interplanetary evolution and global morphology of ICMEs up to Mars distance. Observations from multiple locations are invaluable for space weather studies at Mars and merit more exploration in the future.

Unified Astronomy Thesaurus concepts: Solar coronal mass ejections (310); Space weather (2037); Heliosphere (711)

Supporting material: animations

1. Introduction

Coronal mass ejections (CMEs) are huge eruptions of plasma, magnetic field, and energy that are expelled from the lower solar corona into interplanetary space. The interplanetary coronal mass ejections (ICMEs) are the major cause of severe space weather (Zhang et al. 2007; Shen et al. 2017). ICMEs can cause intense geomagnetic storms at Earth (Zhang et al. 2021b), and can also change the plasma environments of Venus and Mars and increased ion escape rates on those planets (Curry et al. 2015; Dimmock et al. 2018; Zhang et al. 2021a). The capacity to predict the time of ICME arrival before they reach planets is an important aspect of accurate and useful space weather forecasts. During their propagation in the heliosphere, ICMEs can be rotated, distorted, deflected, and decelerated by interacting with the surrounding solar wind (Gopalswamy et al. 2001; Case et al. 2008; Savani et al. 2010; Gui et al. 2011; Temmer et al. 2011; Rollett et al. 2014; Wang et al. 2014; Manchester et al. 2017; Owens et al. 2020). As a result, an accurate understanding of ICME's propagation and dynamic evolution through the heliosphere is of great interest in ICME research and space weather studies.

In situ observations show that ICMEs can be distinguished from the surrounding solar wind by an intense magnetic field, a reasonably monotonic, smooth rotating magnetic field direction, abnormally low proton temperature, decreasing plasma velocity, and lower plasma beta (β; Jian et al. 2006; Richardson & Cane 2010; Chi et al. 2016). For the missions used in the study, which lack dedicated instruments for detecting solar wind plasma, ICMEs may be identified only by their enhanced and smoothly changing magnetic field (Good & Forsyth 2016). Single-point observations have a limited capability of providing information about the general evolution of ICMEs since they are enormous scale structures. In recent years, several

studies have attempted to better understand the structure and evolution of ICMEs by analyzing the ICMEs that are detected in situ by multiple spacecraft (Kilpua et al. 2019; Palmerio et al. 2019; Chi et al. 2020; Salman et al. 2020; Chi et al. 2021; Weiss et al. 2021). However, multiple-point ICME events are relatively rare, due to only a few spacecraft in the inner heliosphere. In addition, most of the spacecraft are located in the sub-1 au heliocentric distances, which constrains the study of overall ICME evolution to 1 au domains.

In this Letter, we expand the investigation of the ICME's evolution to 1.6 au by using the simultaneous measurements by Magnetometer (MAG; Connerney et al. 2015) and the Solar Wind Ion Analyzer (SWIA; Halekas et al. 2015) on board Mars Atmosphere and Volatile EvolutioN (MAVEN; Jakosky et al. 2015b), and the Mars Orbiter Magnetometer (MOMAG; Liu et al. 2020) on board Tianwen-1 (Wan et al. 2020) around Mars. The Tianwen-1 spacecraft is China's first Mars exploration mission, launched on 2020 July 23, to study the environmental characteristics surrounding Mars, from the ionosphere to the solar wind. The Tianwen-1 spacecraft spent 50%–75% of its time (Wang et al. 2023a) in the solar wind. The MOMAG instrument on board the Tianwen-1 spacecraft is a good complement to MAVEN when it is not in the upstream region to monitor the interplanetary magnetic field and to record the passage of huge solar transient structures like ICMEs and stream interaction regions (SIRs).

Chi et al. (2023) identified two ICMEs based on MAVEN/MAG and SWIA data and the first publicly released Tianwen-1/MOMAG data from 2021 December 5 to 2021 December 31. During that time, the BepiColombo (Benkhoff et al. 2021) was located between 0.56 and 0.67 au from the Sun, and the heliocentric separation angle between it and Mars changed from approximately $-16.^{\circ}5$ to 7°. Due to the favorable locations of the BepiColombo and Mars, the two ICMEs were detected by the BepiColombo, MAVEN, and Tianwen-1 spacecraft, offering an excellent opportunity to study the dynamic evolution, expansion, and interaction of the ICMEs with the background solar wind through more than 0.9 au in the heliocentric distance but less than 17° in longitude.

Background-structured solar wind has a significant impact on the evolution of the global morphology of ICMEs as they travel through the heliosphere, which has been confirmed by both observations and modeling (Owens et al. 2006; Savani et al. 2010; Chi et al. 2021). Thus, it is impossible to improve our current knowledge of the dynamic and overall shape evolution of ICMEs without a good understanding of ambient solar wind. In this Letter, we use the Heliospheric Upwind eXtrapolation time (HUXt) model (Owens et al. 2020; Barnard & Owens 2022) to estimate the ambient solar wind conditions in the heliosphere, which uses the Magnetohydrodynamic Algorithm outside a Sphere (MAS) magnetohydrodynamic coronal model (Riley et al. 2001) output as an inner boundary condition. As a surrogate for more comprehensive 3D MHD solar wind models (e.g., HelioMAS), the HUXt model also can be used to simulate the evolution of the global structure of ICMEs and estimate the arrival time of ICMEs to any target of interest in the heliosphere.

In this Letter, we make a comprehensive study of two multipoint observed ICME events and use the model and in situ observations to discuss the evolution of ICMEs during their propagation in the heliosphere up to Mars's distance (1.6 au). This is the first time that BepiColombo has been used as an upstream solar wind monitor of Mars, which highlights that BepiColombo in situ measurements will prove especially useful in monitoring the solar wind upstream of planets in the future to enhance the accuracy of space weather forecasts. Due to the modification of MAVEN's orbit since 2019, the Tianwen-1/MOMAG instrument is currently the only monitor measuring the interplanetary magnetic field at Mars, while Mars Express only measures the density and velocity of the solar wind. In this Letter, the most recent Tianwen-1/MOMAG data released are used to examine the magnetic field properties of Martian ICMEs. To our knowledge, this is one of the first opportunities in which multi-spacecraft studies of the propagation of an ICME up to Mars's distance have been performed, particularly when Earth was not aligned with Mars, which is a very novel approach for Mars space weather. Section 2 presents the data used in the Letter and the analysis of the two ICMEs propagating in the heliosphere. The conclusion and discussion are presented in Section 3.

2. Event Analysis

2.1. Description of the Data

The BepiColombo, which was launched on 2018 October 20, will enter orbit around Mercury in December 2025 after a 7.2 yr voyage. On its way to Mercury, the magnetometer instrument on board the Mercury Planetary Orbiter (MPO-MAG; Glassmeier et al. 2010; Heyner et al. 2021) of the BepiColombo mission can provide in situ measurements of the interplanetary magnetic field. In this Letter, we have used 1 s high-resolution data from the MPO-MAG instrument during 2021 December.

The Tianwen-1 spacecraft is China's first Mars exploration mission. Since 2021 November 16, the MOMAG on board the Tianwen-1 spacecraft has been continuously measuring the local magnetic field conditions around Mars, and its reliability has been verified by Chi et al. (2023) and Zou et al. (2023). The magnetic field data from 2021 November 16 to 2021 December 31 are publicly available from CNSA Data Release System.[11] The MAVEN has been monitoring the solar wind parameters near Mars since 2014 (Jakosky et al. 2015a). The MAG and SWIA on board MAVEN measure the intensity and direction of the interplanetary magnetic field, solar wind density, temperature, bulk flow velocities, and dynamic pressure around Mars.

According to their orbits, the MAVEN and Tianwen-1 spacecraft regularly cross the bow shock and detect the interplanetary solar wind. To rule out the interruptions from measurements taken inside the bow shock, we use the criteria described by Wang et al. (2023a) to confirm the interval between Tianwen-1 entering the solar wind from the magnetic sheath and the time the solar wind entered the magnetic sheath. Based on observations of the solar wind speed $|v| > 200$ km/s, normalized magnetic field fluctuation levels $\sigma B/|B| < 0.15$, altitude $R > 500$ km, and $\sqrt{(T/|v|)} < 0.012$ (Halekas et al. 2017), the selection criteria for MAVEN's undisturbed solar wind periods are determined.

The remote sensing observations of the Sun are from the C2/C3 coronagraph observations of the SOlar and Heliospheric Observatory (SOHO)/the Large Angle and Spectrometric COronagraph (LASCO; Brueckner et al. 1995), as well as the COR2 observations of the Solar TErrestrial Relations Observatory Ahead (STEREO-A; Kaiser et al. 2008)/Sun Earth

[11] http://202.106.152.98:8081/marsdata/

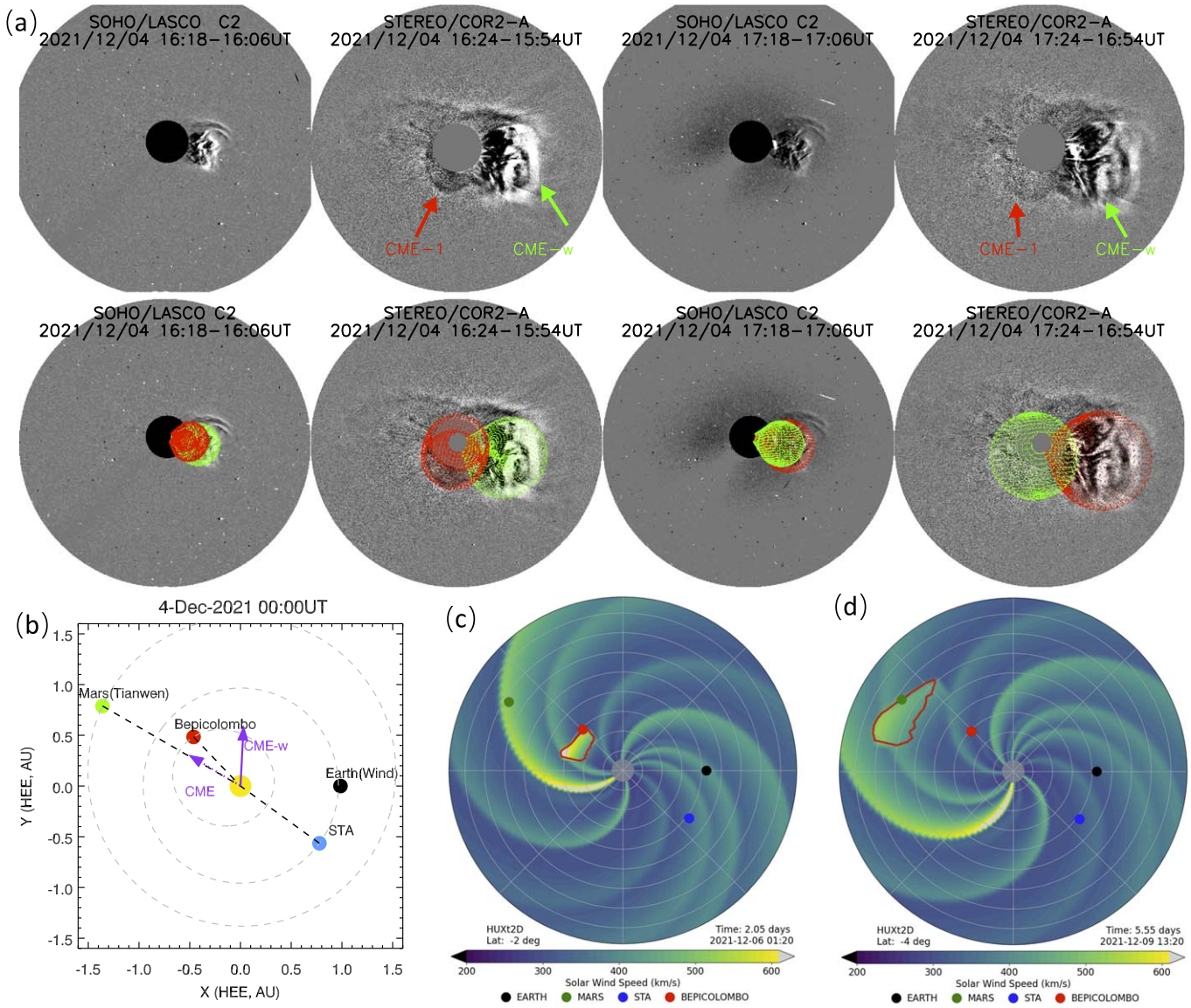

Figure 1. Panel (a) shows the running difference images of CMEs and the GCS fitting results from SOHO/LASCO/C3 and SECCHI/COR2-A at 16:24UT and 17:18UT on 2021 December 4 from left to right, respectively. The red and green meshes in the lower panels display the results of the GCS fitting for CME-1 and CME-w, respectively. Panel (b) shows the position of Mars, STEREO-A, and Earth in Heliocentric Earth Ecliptic (HEE) coordinates on 2021 December 4. The lavender arrows indicate the propagation direction of CME-1 and CME-w determined from the GCS model. The black dot, green dot, blue dot, and red dot show the positions of Earth, Mars, STEREO-A, and BepiColombo, respectively. Panels (c), (d) show snapshots of the solar wind as the ICME impacts the BepiColombo and Mars on the solar equatorial plane, as simulated by the HUXt model. The red lines in panels (c), (d) mark the boundaries of ICME-1. An animation of panels (c), (d) is available, showing the evolution of CME-1 boundary by interacting with the ambient solar wind. It covers 9.96 days starting at 00:08 on 2021 December 4. The real-time duration of the animation is 20 s.

(An animation of this figure is available.)

Connection Coronal and Heliospheric Investigation (SECCHI; Howard et al. 2008) instrument suite.

2.2. The 2021 December 4 ICME

On December 10, Tianwen-1 and MAVEN identified the first ICME event near Mars that lasted approximately 28 hr and featured an increased magnetic field, smoothly changing magnetic field directions, lowered plasma velocity, and reduced plasma beta. According to the maximal velocity of this ICME at Mars (539.41 km s^{-1}), the parent ICME should have erupted about 5.33 days before the arrival of the ICME. We searched for potential parent CMEs in a 3 day continuous window around December 4, using running difference observations from SOHO/LASCO and STEREO-A/COR2. As shown in Figure 1(b), Mars is located at 1.66 au and has a separation angle with Earth of 149°.88 with STEREO-A of 174°.38 on December 4. The satellite and planet's relative positions indicate that the parent CME should be ejected from the back side of the Sun relative to observers and show as a halo or partial halo CME in the field of view of STEREO-A/COR2 and SOHO/LASCO. In the search window, STEREO-A/COR2 only observed one back-side partial halo CME. As shown in Figure 1(a), the red arrows in the first row present the parent CME (CME-1) in the running difference images of STEREO-A/COR2. A westward CME was also noticed at the same time in LASCO/field C3's of view. However, it is confirmed that this westward CME does not match the back-

Table 1
CME Input Parameters Specified for the HUXt Model and Predicted Arrival Times at the BepiColombo and Mars

CME Initial Parameters						BepiColombo		Mars	
Time (UT)	Longitude (deg)	Latitude (deg)	Half Angle (deg)	Height ($R_\odot$)	Speed (km s^{-1})	Predicted Arrival Time (UT)	Actual Arrival Time (UT)	Predicted Arrival Time (UT)	Actual Arrival Time (UT)
2021-12-04 17:39	149(±5)	−11(±5)	43.6(±10)	17.55(±2)	761.2(±50)	2021-12-06 18:25(+3.5/−3)	2021-12-06 15:07	2021-12-10 07:50(+7/−5.5)	2021-12-08 19:20
2022-12-22 00:38	148(±5)	1.8(±5)	36.5(±10)	15.91(±2)	390.7(±50)	2021-12-24 21:17(+7/−6)	2021-12-24 18:52	2021-12-28 23:28(+10/−14)	2021-12-29 00:00

side parent CME; rather, it matches another CME (CME-w), as shown by the green arrows in the FOV of STEREO-A/COR2. In the field of view (FOV) of LASCO/C2, the brilliant structure of CME-w makes it difficult to identify the corresponding signature of CME-1. According to the relative positions of Mars and STEREO-A, the heliospheric imagers on board STEREO-A cannot be used to follow the two CMEs.

To reconstruct the propagation direction and initial velocity of the two CMEs, we apply the graduated cylindrical shell (GCS) model (Thernisien et al. 2006, 2009) to nearly simultaneous images from STEREO-A/COR2 and SOHO/LASCO. The lack of CME-1 signatures in the FOV of SOHO/LASCO makes it difficult to determine six unambiguous parameters in the GCS model. By assuming that the initial CME form was spherical, we simplified the GCS model to a GCS cone model (Palmerio et al. 2019). The GCS cone model is uniquely determined by four parameters: longitude, latitude, half angle, and height. The second row in Figure 1(a) shows the GCS cone fitting overlaid on running difference images produced from observations made by LASCO/C3 and STEREO/COR2-A for CME-1 (red mesh) and CME-w (green mesh) at two different times. CME-1's best-fit propagation direction was longitude $149° \pm 5°$ and latitude $-11° \pm 5°$ in HEEQ coordinate, which was nearly directly at Mars (only 1° east of the CME apex direction). The GCS model determined CME-w's initial longitude to be 87°, close to quadrature to Earth. The propagation directions of CME-1 and CME-w are indicated by the purple arrows in Figure 1(b).

The BepiColombo was located at 0.67 au and at 133°.67 longitude, 16°.2 east of Mars, marked as a red dot in Figure 1(b). Due to the favorable locations of the BepiColombo, it has more than 49% possibility to detect ICME-1 (Good & Forsyth 2016). We use the HUXt model in this study to forecast whether the ICME will hit the spacecraft, as well as the arrival time and velocity, and compare it to in situ data at the target of interest. Table 1 shows the initial ICME-1 parameters derived from the GCS cone model and utilized in the HUXt model. The HUXt model solution is shown in Figure 1(c), (d), including the locations of ICME-1 and the ambient solar wind, as well as the relative positions of the spacecraft and planets on the ecliptic plane. As illustrated in Figure 1(c), the west flank of ICME-1 impacted the BepiColombo, with a predicted arrival time of December 6, 18:25 UT. Figure 2(a) shows the magnetic field in situ observations from the BepiColombo. The black, red, green, and blue lines represent the total magnetic field as well as the r, t, and n component magnetic field in RTN coordinates. At 15:07 UT on 2021 December 6, a clear shock structure was detected by the BepiColombo as shown by the vertical lavender line in panel (a). After 7 hr, the BepiColombo magnetic field data show a magnetic obstacle arrival between 22:23 UT on December 6 and 13:50 UT on December 7 (lavender shadow in panel (a)). The predicted arrival time of this ICME is shown by the red vertical line about 3 hr later than the in situ observations. When forecasting ICME arrival time at Earth, Riley et al. (2018) found that the typical error of predicting ICME-shock arrival times within ± 10 hr. Thus, the differences between the actual and predicted arrival times of ICME within 3 hr are a very good match and suggest the ICME is indeed the same structure seen in situ.

Mars is located only 1° east of the ICME apex direction obtained from the GCS model. Because the BepiColombo recorded a clear shock ahead of the ICME, we expect that MAVEN and Tianwen-1 in situ observations will likely identify an ICME event with shock. Figure 2(b) shows the magnetic field and solar wind in situ observations from MAVEN and Tianwen-1. From top to bottom, the parameters are the total magnetic field intensity (B), the elevation (θ) and azimuthal (ϕ) angles of magnetic field direction in the Mars-centered Solar Orbital (MSO) coordinate system, three components of the magnetic field in the MSO coordinate system (B_x, B_y, and B_z) from MAVEN/MAG (black asterisks) and Tianwen-1/MOMAG (red asterisks), the solar wind speed, plasma density, total dynamic pressure, proton temperature, and plasma beta from MAVEN/SWIA. No clear shock was detected by MAVEN and Tianwen-1 in situ observations. Due to the fact that only a portion of MAVEN and Tianwen-1's orbits was beyond the bow shock and extended into the solar wind, the shock's signatures may not be detected noticeably close to Mars. According to the peak dynamic pressure that may be associated with the shock arrival, we found a potentially related fast-forward shock (lavender vertical line in panel (b)) discovered by Tianwen-1 and MAVEN spacecraft at around 19:20 UT on 2021 December 8. The lavender-shaded region in panel (b) indicates the interval of the ICME, from 00:00 UT on December 10 to 14:10 UT on December 11. The discrepancy between the predicted arrival time from the HUXt model (red vertical line) and the actual arrival time (lavender vertical line) at Mars is about 38 hr. The blue line in panel (b) shows the simulated solar wind velocity with the ICME calculated from the HUXt model. The simulated velocity profile is similar to the in situ observations at Mars but with a time lag of several hours.

The average transit velocities of the ICME to the two observation points are estimated using the observers' heliocentric distances, the initial time of the CME input into the HUXt model, and the in situ observed time listed in Table 1. The average transit velocity of the ICME between the Sun and

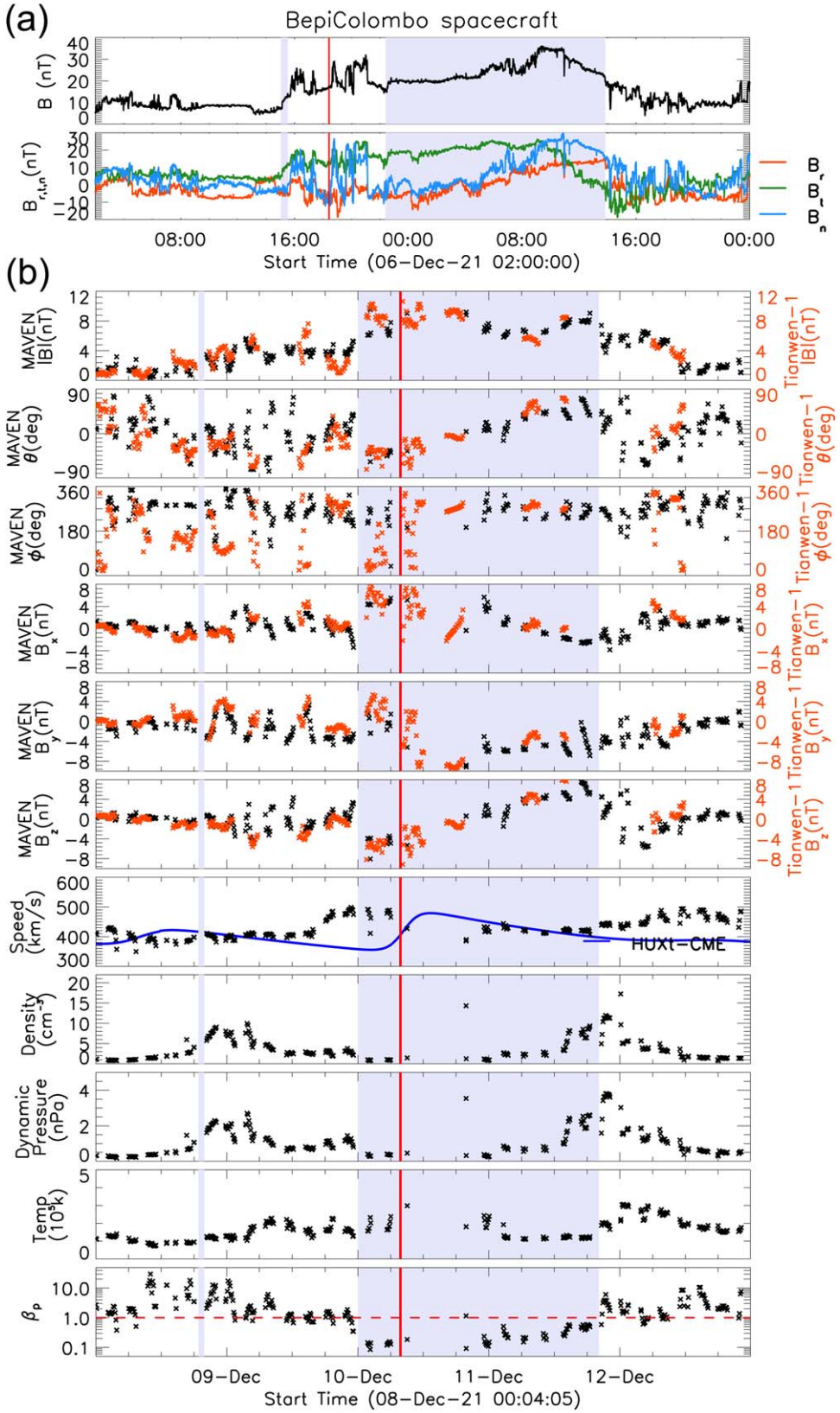

Figure 2. Panel (a) shows the magnetic field strength and the r, t, n components in the RTN coordinate of ICME-1 at BepiColombo. The lavender vertical line and lavender shaded area represent indicate the arrival of the shock and interval of ICME-1. The red vertical line shows the predicted arrival time of ICME-1. Panel (b) shows Tianwen and MAVEN spacecraft in situ observations of a 5 day time interval starting from 00:04UT on 2021 December 8. From top to bottom, these panels are the magnetic field strength (B), the elevation (θ) and azimuthal (ϕ) angles of the magnetic field in the MSO coordinate system, three components of the magnetic field in the MSO coordinate system (B_x, B_y, and B_z) from MAVEN/MAG (black asterisks) and Tianwen-1/MOMAG (red asterisks), solar wind speed (V_{sw}), proton density (N_p), the total pressure(P_{dp}), proton temperature (T_p), and plasma beta (β) from MAVEN/SWIA. The blue solid line represents the simulated solar wind velocity with the ICME calculated from the HUXt model. The lavender vertical line and lavender shaded area represent the shock caused by the ICME and interval corresponding to the ICME determined from the data, while the red vertical line indicates the projected arrival time from the HUXt model.

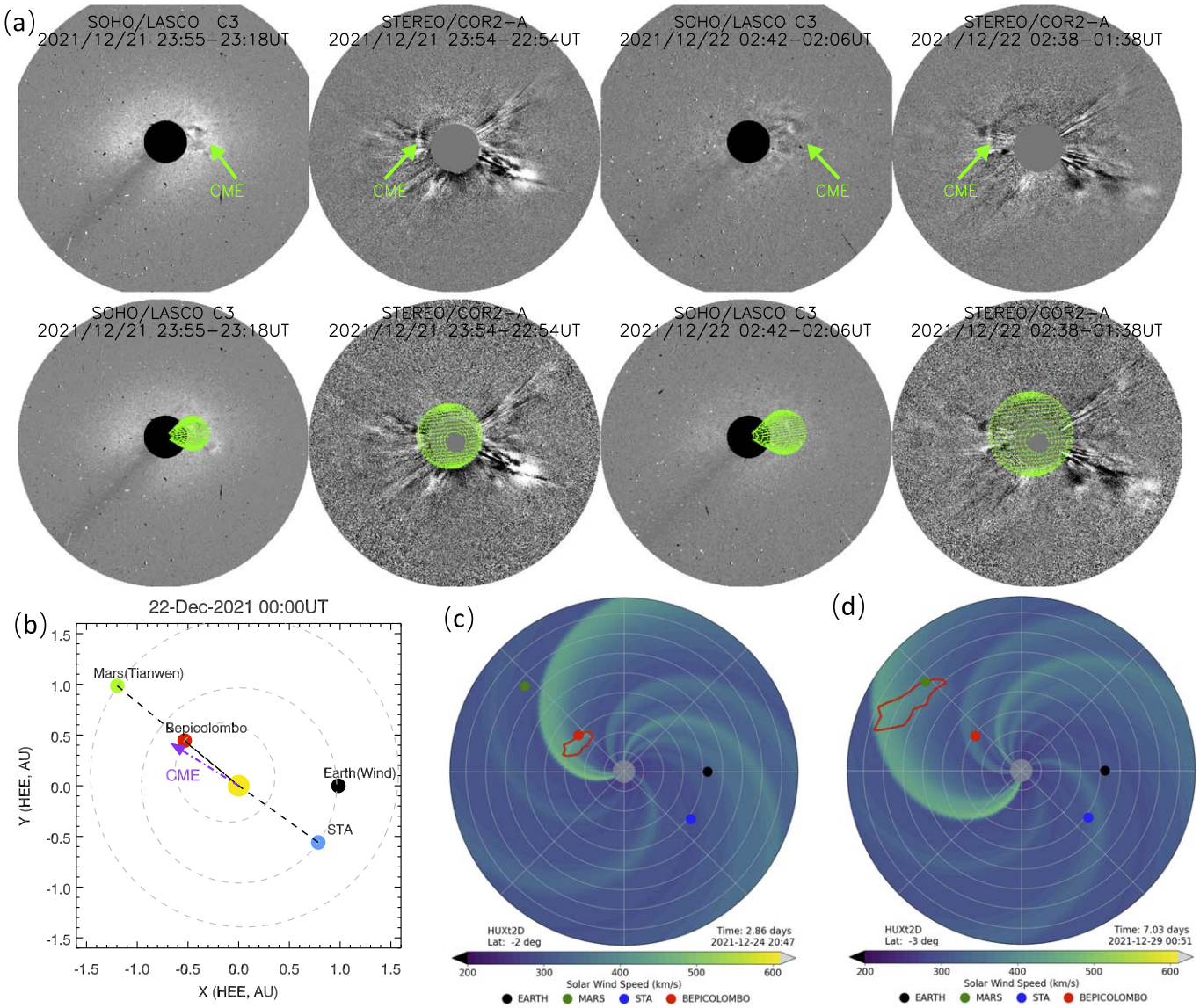

Figure 3. The plot setup is the same as in Figure 1 but for the CME-2. An animation of panels (c), (d) is available. The animation begins on 2021 December 22 at 00:08 and ends 9.96 days later on 2021 December 31 at 23:17. The real-time duration of the animation is 20 s.

(An animation of this figure is available.)

BepiColombo (0.67 au) is 611.90 km s^{-1}, while it is 702.45 km s^{-1} between the Sun and Mars (1.66 au). The transit velocity of the ICME at 0.67 au is smaller than that at 1.66 au, which differs from the expected average transit speeds. The discrepancy could be due to the longitudinal separation of the two in situ observers and the distortion of the ICME by the structured solar wind. As the BepiColombo is located 16°.2 west of Mars, it detected the west flank of the ICME. Figure 1 panel (c) shows the background solar wind speed in the solar equatorial plane and the position of the ICME. As shown in HUXt model animation associated with Figure 1, the west flank of ICME-1 encounters the slow solar wind ($\leqslant$300km s^{-1}), while the east part of the ICME is in the fast solar wind ($\geqslant$600 km s^{-1}). As CMEs are not coherent structures (Owens et al. 2017) during their propagation in the heliosphere, they can be distorted when different segments of a CME encounter different velocity regimes within a structured solar wind (Owens et al. 2006; Chi et al. 2021). Thus, we expect that the CME front should be strongly distorted during its propagation.

2.3. The 2021 December 22 ICME

According to Chi et al. (2023), the second ICME identified by Tianwen-1 and MAVEN occurs between 00:00 UT on 2021 December 29 and 20:00 UT on 2021 December 30. As shown in Figure 4(b), the velocity of this ICME at Mars is relatively slow. The in situ measured front velocity of this slow ICME is only 353.46 km s^{-1} as a result of a long transit time of approximately 7 days from its eruption to Mars. Based on that, we estimate that the corresponding CME should erupt around 2021 December 22. STEREO-A should detect the CME as a back-side halo or partial halo CME since it was situated on the opposite side of Mars from the Sun (176°.0 east of Mars) during that time. As the projected propagation speed of this CME is quite slow, we prefer to use large time running differences to search for the parent CME in a 3 day long continuous window of SOHO/LASCO and STEREO/C2 observations. Figure 3(a) shows white light images taken by the SOHO/LASCO and STEREO-A/COR2 on 2021 December 21 at 23:54 UT (two

left columns) and 2021 December 22 at 02:40 UT (two right columns). The CME erupted as a weak CME from the Sun's western limb as seen by SOHO/LASCO and as a faint halo CME in the FOV of STEREO/COR2. The back-side, fainter CME darkens faster, making it impossible to be detected for a longer period of time. We fitted the coronagraph observations of the CME with the GCS cone model, which results in a direction of $148 \pm 5°$ longitude and $1\overset{\circ}{.}8 \pm 5°$ latitude in the HEEQ coordinate.

The BepiColombo was positioned at 0.69 au and $140\overset{\circ}{.}11$ longitude, while Mars was located at 1.55 au and $140\overset{\circ}{.}53$ longitude, as indicated in Figure 3(b). The angle of separation between the BepiColombo and Mars is only $0\overset{\circ}{.}44$. It is an excellent opportunity to study the propagation of the ICME at the same longitude. The CME apex direction obtained from the GCS model is $148° \pm 5°$ in longitude. Table 1 shows the parameters of this CME obtained from the GCS cone model, which was input into the HUXt model. The apex of the CME is 8° deviating from the position of the BepiColombo. Panels (c), (d) in Figure 3 show the global configuration of the ICME at its predicted arrival time at BepiColombo and Mars, which are also provided in Table 1 and are highlighted by red vertical lines in Figure 4(a), (b). Even though the velocity of this ICME is very slow, a clear shock (lavender vertical line in Figure 4(a)) was detected by BepiColombo ahead of the corresponding ICME (lavender region) with a clear enhancement of the magnetic field. The first detection of the ICME at the BepiColombo was at 18:52 UT on December 24, only less than 2.5 hr earlier than the predicted arrival time of this ICME (21:17 UT on December 24) computed by the HUXt model.

Figure 4(b) shows the in situ observations from Tianwen-1 and MAVEN at Mars. Here we use the same interval of ICME from Chi et al. (2023). The lavender shadow region shows the interval of ICME from 00:00UT on December 29 to 20:00UT on December 30. The detection time of the ICME is approximately half an hour later than the predicted arrival time (23:28 on December 29) by the HUXt model at Mars. Unlike the observations from the BepiColombo, no clear shock was detected by MAVEN and Tianwen-1 in situ observations. Not only is there no discernible enhancement in the magnetic field, but there is also no trace of plasma density or dynamic pressure. This indicates that the shock ahead of the ICME may dissipate from the BepiColombo to Mars due to the momentum exchange with the ambient solar wind (Luhmann 1995).

The initial velocity of the slow ICME derived from the GCS model is $390.7(\pm 50)\,\mathrm{km\,s^{-1}}$. The average velocity of the ICME from its eruption to 0.69 au (position of BepiColombo) is $432.91\,\mathrm{km\,s^{-1}}$, slightly faster than the initial velocity. The HUXt model animation (see the animations associated with Figure 3) demonstrates that the slow ICME propagates in the rear of a region of fast solar wind. It indicates that the velocity of slow ICMEs undergoes a gradual acceleration to the average solar wind level from its eruption to 0.69 au (Liu et al. 2013; Salman et al. 2020). The ICME's average transit speed from the BepiColombo to Mars is $353.37\,\mathrm{km\,s^{-1}}$, which exactly matches the in situ measured front speed of $353.36\,\mathrm{km\,s^{-1}}$ around Mars, and the in situ measured and the simulated velocities (blue line) of the slow ICME are comparable to the ambient solar wind at Mars. This supports the argument that the acceleration/deceleration of slow ICMEs extends to only approximately 0.69 au (Gopalswamy et al. 2001; Winslow et al. 2015).

3. Discussions and Conclusions

To analyze CME evolution in the heliosphere, this Letter presents a detailed study of two ICME events measured by the Tianwen-1, MAVEN, and BepiColombo, combining the white light observations from SOHO and STEREO-A, and with the 3D HUXt model. BepiColombo is used for the first time to monitor Mars's upstream solar wind, and Tianwen-1/MOMAG is used for the first time to study the magnetic field characteristics of ICMEs at Mars. Even without the heliospheric observations, the multipoint in situ observations provide an excellent opportunity to test the CME propagation model and better understand the evolution of CME dynamics and global shape.

The results show that the background solar wind plays an important role in determining the interplanetary evolution and global morphology of CMEs. The average transit velocity of CME-1 from its eruption to BepiColombo (0.67 au) is $611.90\,\mathrm{km\,s^{-1}}$, which is less than the average transit velocity of $702.45\,\mathrm{km\,s^{-1}}$ to Mars (1.66 au; longitudinal separations:$16\overset{\circ}{.}2$). The analysis of this event provides additional evidence that the front of the CME can be strongly distorted when different segments of a CME encounter different velocity solar wind (Owens et al. 2006; Chi et al. 2021). The differences between predicted and actual ICME arrival times at two separate positions show that the global shape of ICME-1 is more distorted than the HUXt modeling result. It suggests that the actual ambient solar wind is more complicated than the simulation. Using the data assimilation technique (Lang & Owens 2019; Lang et al. 2021) to establish a more accurate ambience-structured solar wind will enhance the model's capability to predict ICME arrival timing and speed.

The background solar wind also plays an important role in determining the dynamic evolution of CMEs. When the second slow CME erupted, the longitudinal separation between the BepiColombo and Mars was only $0\overset{\circ}{.}43$. Thus, we can study the dynamic evolution of the CME at the same longitude, eliminating the effect of the CME distortion. The study shows that the slow CME undergoes an acceleration from 15.91 $R_\odot$ to 0.69 au and drives a clear shock ahead of the ejecta. It confirmed that slow ICME also can drive a shock ahead of it (Lugaz et al. 2017). The ICME's average transit speed from the BepiColombo to Mars exactly matches the in situ measured front speed around Mars. It indicates that the acceleration/deceleration of slow ICME stops at somewhere in 0.69 au and then travels with constant velocity. The predicted arrival time of the slow ICME is consistent with the actual observations from BepiColombo, Tianwen-1, and MAVEN (discrepancies less than 2.5 hr). It indicates that for these two particular events, even without the heliospheric observations, the coronal observations and the model can accurately predict the arrival time of the ICME.

It should be noted that the HUXt model includes a uniform acceleration (Owens et al. 2020), which has a direct impact on the distortion of the CME in the model, and the estimation of arrival times. The acceleration was first induced by Riley & Lionello (2011) in order to best match the acceleration profile of full MHD models between 30 R and 1 au. Bunting & Morgan (2023) compared the OMNI, STEREO-A, and STEREO-B observational data with the model results, demonstrating the HUXt model is almost as accurate as MHD model but considerably easier to implement (Riley & Issan 2021). While the parameters governing the acceleration are

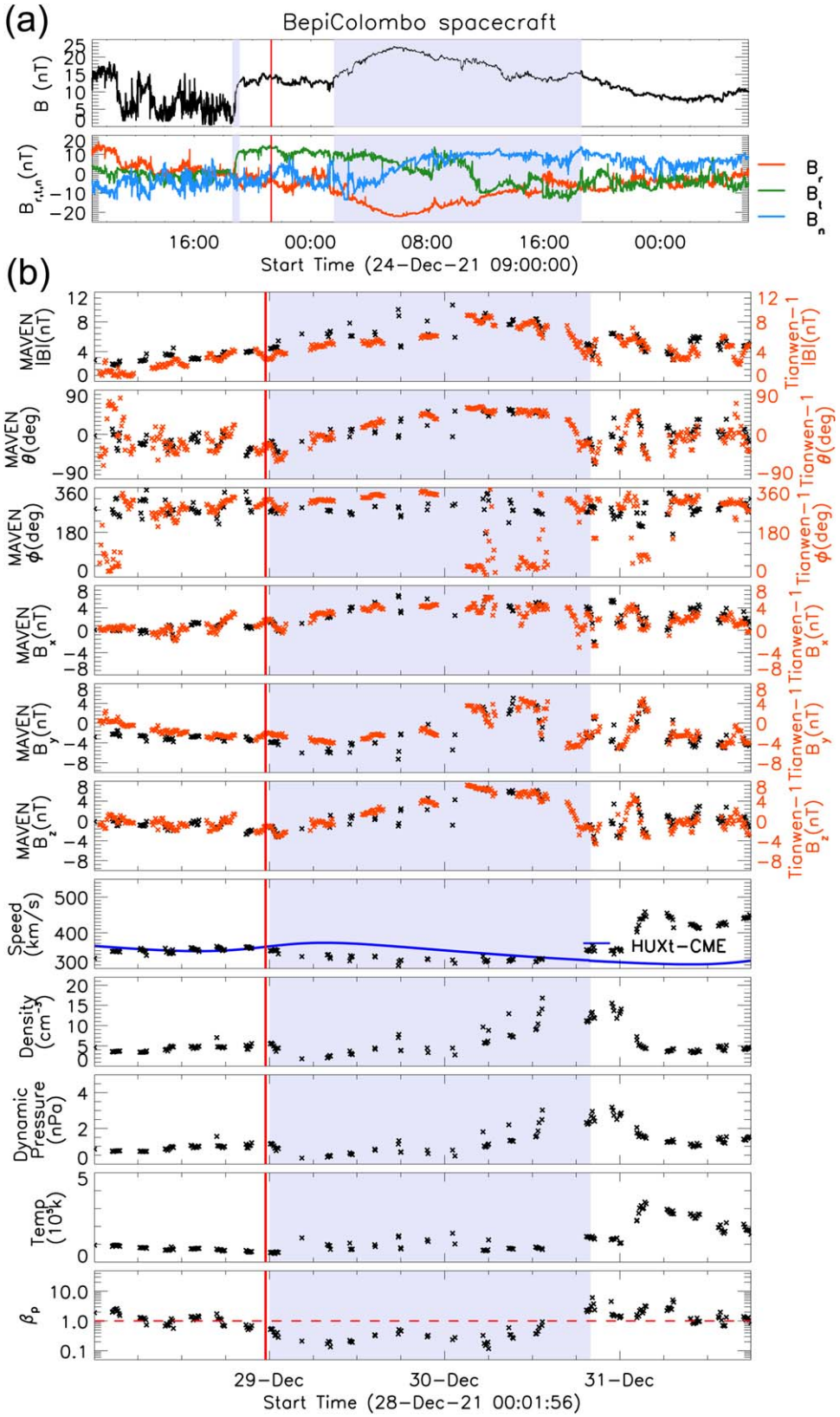

Figure 4. Panel (a) shows the magnetic field measurements of the ICME at BepiColombo. Panel (b) shows Tianwen and MAVEN spacecraft in situ observations of a 4 day time interval starting from 00:01UT on 2021 December 28. The plot setup is the same as in Figure 2.

fixed, the acceleration is not actually constant—it varies with distance and solar wind speed to closely mimic polytropic MHD. Using PSP data to model solar wind conditions at distances much closer than 1 au will be helpful to do a more in-depth investigation of solar wind acceleration in the future.

The accuracy of ICME arrival times can be affected by uncertainties in the CME initial conditions. The initial

parameters of the two CMEs estimated from the GCS model contain uncertainty due to the unclear signatures of the two CMEs in the coronagraph imagers from SOHO and STEREO-A. According to Thernisien et al. (2009), the uncertainty of the CME's initial parameters obtained by GCS model are $\pm5°$ in longitude and latitude, $\pm10°$ in half angle, $\pm50 km s^{-1}$ in initial velocity, and $\pm2R_{\odot}$ in initial height. We create 200 ensemble members, which are used as inputs into HUXt model and described by various GCS parameters (200 random values in the uncertainty range; Barnard et al. 2020; Owens et al. 2020). Table 1 displays the uncertainty of the two ICMEs' arrival times at BepiColombo and Mars according to the uncertainty in CME initial conditions. The detailed description of the ensemble model can be found in Mays et al. (2015). The ensemble arrival time distribution spans for the fast ICME are about 6.5 hr at BepiColombo and 12.5 hr at Mars, which are smaller than those for slow ICME (13 hr at BepiColombo and 24 hr at Mars). It indicates that accurate ICME initial parameters are crucial in predicting the slow ICMEs' arrival time.

According to BepiColombo in situ observations, the first fast ICME, as well as the second slow ICME, both produced a clear shock ahead of them, identified by abrupt increases in the magnetic field magnitude. However, no clear shock was detected by Tianwen-1 and MAVEN near Mars. For the first fast ICME, we still can identify a shock signal with enhanced plasma density and dynamic pressure. For the second slower ICME, no clear shock signal was detected by Tianwen-1 and MAVEN. Therefore, we may conclude that the shock underwent a process of dissipation from 0.67 to 1.56 au by changing momentum with the surrounding solar wind.

It is necessary to conduct statistical analyses of ICME events with multiple observations since it is known that individual event studies do not reveal global trends. With the launch of Solar Orbiter (Müller et al. 2020), Parker Solar Probe (Fox et al. 2016), the future Vigil mission (Luntama et al. 2020), and the future solar ring mission (Wang et al. 2020, 2023b), we are entering a new era of inner heliosphere exploration from multi-spacecraft in situ observations. The in situ and remote observations of CMEs at various radial distances provide a fantastic chance to analyze the radial evolution of CME dynamics, magnetic fields, and ICME interactions with other structures.

Acknowledgments

All Tianwen-1 magnetic field data are available through the Planet Exploration Program Scientific Data Release System (http://202.106.152.98:8081/marsdata/), or the data used in the paper can be directly downloaded from the official website of the MOMAG team (http://space.ustc.edu.cn/dreams/tw1_momag/). All MAVEN data used in this paper are available from NASA's Planetary Data System (https://pds-ppi.igpp.ucla.edu/mission/MAVEN/MAVEN/). We would like to thank the entire BepiColombo/MPO-MAG team for providing data access and support. Although the data have not yet been made public, they can be obtained by contacting the principal investigator, D. Heyner. Direct download links for the BepiColombo/MPO-MAG data used in the study can be found at doi:10.25392/leicester.data.22203376.v1. We acknowledge the use of data from the SOHO and STEREO spacecraft. STEREO is the third mission in NASA's Solar Terrestrial Probes program. SOHO is a project of international cooperation between the ESA and NASA.

This work is supported by grants from the NSFC (42130204, 41904151, 42188101, 42074222), the Strategic Priority Program of the Chinese Academy of Sciences (XDB41000000) and the CNSA pre-research Project on Civil Aerospace Technologies (Grant D020104). B.S-C. acknowledges support through UK-STFC Ernest Rutherford Fellowship ST/V004115/1 and ST/V000209/1. D.H., H.U.A. and I.R. were supported by the German Ministerium für Wirtschaft und Klimaschutz and the German Zentrum für Luft-und Raumfahrt under contract 50QW2202.

ORCID iDs

Yutian Chi https://orcid.org/0000-0001-9315-4487
Chenglong Shen https://orcid.org/0000-0002-3577-5223
Junyan Liu https://orcid.org/0009-0006-7051-0438
Zhihui Zhong https://orcid.org/0000-0002-5627-2377
Mathew Owens https://orcid.org/0000-0003-2061-2453
Christopher Scott https://orcid.org/0000-0001-6411-5649
Luke Barnard https://orcid.org/0000-0001-9876-4612
Bingkun Yu https://orcid.org/0000-0003-2758-1960
Ingo Richter https://orcid.org/0000-0002-5324-4039
Yuming Wang https://orcid.org/0000-0002-8887-3919
Jingnan Guo https://orcid.org/0000-0002-8707-076X
Beatriz Sánchez-Cano https://orcid.org/0000-0003-0277-3253
Zhuxuan Zou https://orcid.org/0009-0008-9920-9600
Mengjiao Xu https://orcid.org/0000-0002-2924-7520
Long Cheng https://orcid.org/0000-0003-0578-6244
Zhenpeng Su https://orcid.org/0000-0001-5577-4538
Can Wang https://orcid.org/0000-0002-2865-4626
Guoqiang Wang https://orcid.org/0000-0002-6618-4928
Kai Liu https://orcid.org/0000-0003-2573-1531
Mike Lockwood https://orcid.org/0000-0002-7397-2172

References

Barnard, L., & Owens, M. 2022, FrP, 10, 1062
Barnard, L., Owens, M. J., Scott, C. J., & de Koning, C. A. 2020, AGUA, 1, e2020AV000214
Benkhoff, J., Murakami, G., Baumjohann, W., et al. 2021, SSRv, 217, 1
Brueckner, G., Howard, R., Koomen, M., et al. 1995, in The SOHO Mission, ed. B. Fleck, V. Domingo, & A. Poland (Dordrecht: Springer), 357
Bunting, K. A., & Morgan, H. 2023, SpWea, 21, e2023SW003448
Case, A., Spence, H. E., Owens, M., Riley, P., & Odstrcil, D. 2008, GeoRL, 35, 15
Chi, Y., Scott, C., Shen, C., et al. 2020, ApJ, 899, 143
Chi, Y., Scott, C., Shen, C., et al. 2021, ApJL, 917, L16
Chi, Y., Shen, C., Cheng, L., et al. 2023, ApJS, in press (arXiv:2303.07078)
Chi, Y., Shen, C., Wang, Y., et al. 2016, SoPh, 291, 2419
Connerney, J., Espley, J., Lawton, P., et al. 2015, SSRv, 195, 257
Curry, S. M., Luhmann, J. G., Ma, Y. J., et al. 2015, GeoRL, 42, 9095
Dimmock, A. P., Alho, M., Kallio, E., et al. 2018, JGRA, 123, 3580
Fox, N., Velli, M., Bale, S., et al. 2016, SSRv, 204, 7
Glassmeier, K.-H., Auster, H.-U., Heyner, D., et al. 2010, P&SS, 58, 287
Good, S., & Forsyth, R. 2016, SoPh, 291, 239
Gopalswamy, N., Lara, A., Yashiro, S., Kaiser, M. L., & Howard, R. A. 2001, JGRA, 106, 29207
Gui, B., Shen, C., Wang, Y., et al. 2011, SoPh, 271, 111
Halekas, J., Ruhunusiri, S., Harada, Y., et al. 2017, JGRA, 122, 547
Halekas, J., Taylor, E., Dalton, G., et al. 2015, SSRv, 195, 125
Heyner, D., Auster, H.-U., Fornaćon, K.-H., et al. 2021, SSRv, 217, 1
Howard, R. A., Moses, J., Vourlidas, A., et al. 2008, SSRv, 136, 67
Jakosky, B. M., Grebowsky, J. M., Luhmann, J. G., & Brain, D. A. 2015a, GeoRL, 42, 8791
Jakosky, B. M., Lin, R. P., Grebowsky, J. M., et al. 2015b, SSRv, 195, 3
Jian, L., Russell, C., Luhmann, J., & Skoug, R. 2006, SoPh, 239, 393

Kaiser, M. L., Kucera, T., Davila, J., et al. 2008, SSRv, 136, 5
Kilpua, E. K. J., Good, S., Palmerio, E., et al. 2019, FrASS, 6, 50
Lang, M., & Owens, M. J. 2019, SpWea, 17, 59
Lang, M., Witherington, J., Turner, H., Owens, M. J., & Riley, P. 2021, SpWea, 19, e02698
Liu, K., Hao, X., Li, Y., et al. 2020, E&PP, 4, 384
Liu, Y. D., Luhmann, J. G., Lugaz, N., et al. 2013, ApJ, 769, 45
Lugaz, N., Farrugia, C. J., Winslow, R. M., et al. 2017, ApJ, 848, 75
Luhmann, J. 1995, AdSpR, 15, 355
Luntama, J.-P., Kraft, S., & Glover, A. 2020, in 100th American Meteorological Society Annual Meeting, AMS, https://ams.confex.com/ams/2020Annual/meetingapp.cgi/Paper/370660
Manchester, W., Kilpua, E. K., Liu, Y. D., et al. 2017, SSRv, 212, 1159
Mays, M., Taktakishvili, A., Pulkkinen, A., et al. 2015, SoPh, 290, 1775
Müller, D., Cyr, O. S., Zouganelis, I., et al. 2020, A&A, 642, A1
Owens, M., Lang, M., Barnard, L., et al. 2020, SoPh, 295, 1
Owens, M., Lockwood, M., & Barnard, L. 2017, NatSR, 7, 4152
Owens, M. J., Merkin, V., & Riley, P. 2006, JGRA, 111, A03104
Palmerio, E., Scolini, C., Barnes, D., et al. 2019, ApJ, 878, 37
Richardson, I. G., & Cane, H. V. 2010, SoPh, 264, 189
Riley, P., & Issan, O. 2021, FrP, 9, 268
Riley, P., Linker, J., & Mikić, Z. 2001, JGRA, 106, 15889
Riley, P., & Lionello, R. 2011, SoPh, 270, 575
Riley, P., Mays, M. L., Andries, J., et al. 2018, SpWea, 16, 1245
Rollett, T., Möstl, C., Temmer, M., et al. 2014, ApJL, 790, L6
Salman, T., Winslow, R. M., & Lugaz, N. 2020, JGRA, 125, e27084
Savani, N. P., Owens, M. J., Rouillard, A., Forsyth, R., & Davies, J. 2010, ApJL, 714, L128
Shen, C., Chi, Y., Wang, Y., Xu, M., & Wang, S. 2017, JGRA, 122, 5931
Temmer, M., Rollett, T., Möstl, C., et al. 2011, ApJ, 743, 101
Thernisien, A., Howard, R., & Vourlidas, A. 2006, ApJ, 652, 763
Thernisien, A., Vourlidas, A., & Howard, R. 2009, SoPh, 256, 111
Wan, W., Wang, C., Li, C., & Wei, Y. 2020, NatAs, 4, 721
Wang, Y., Ji, H., Wang, Y., et al. 2020, Sci. China: Technol. Sci., 63, 1699
Wang, Y., Wang, B., Shen, C., Shen, F., & Lugaz, N. 2014, JGRA, 119, 5117
Wang, Y., Zhang, T., Wang, G., et al. 2023a, E&PP, 7, 1
Wang, Y., Bai, X., Chen, C., et al. 2023b, AdSpR, 71, 1146
Weiss, A. J., Möstl, C., Davies, E., et al. 2021, A&A, 656, A13
Winslow, R. M., Lugaz, N., Philpott, L. C., et al. 2015, JGRA, 120, 6101
Zhang, C., Rong, Z., Nilsson, H., et al. 2021a, ApJL, 922, L33
Zhang, J., Temmer, M., Gopalswamy, N., et al. 2021b, PEPS, 8, 56
Zhang, J., Richardson, I., Webb, D., et al. 2007, JGRA, 112, A10102
Zou, Z., Wang, Y., Zhang, T., et al. 2023, Sci. China: Technol. Sci., in press